# Supporting Information

## Enhancing direct hydroxylation of benzene to phenol on $Fe_1$/PMA single-atom catalyst: a comparative study of $H_2O_2$ vs. $O_2$-assisted reactions

Beenish Bashir[a, b], Shamraiz Hussain Talib[c, d], Muhammad Ajmal Khan[b], Sharmarke Mohamed[c, d] Ahsan Ulhaq Qurashi[c, d], Hai Xiao[a] and Jun Li[a, e, *]

[a]Department of Chemistry and Engineering Research Center of Advanced Rare-Earth Materials of Ministry of Education, Tsinghua University, Beijing 100084, China

[b]Department of Chemistry and Biochemistry, George Mason University, 4400 University Drive, Fairfax, VA 22030, USA.

[c]Advanced Materials Chemistry Centre (AMCC), SAN Campus, Khalifa University, Abu Dhabi, P.O. Box 127788, United Arab Emirates

[d]Department of Chemistry, Khalifa University of Science and Technology, Abu Dhabi 127788, United Arab Emirates

[e]Department of Chemistry, Southern University of Science and Technology, Shenzhen 518055, China

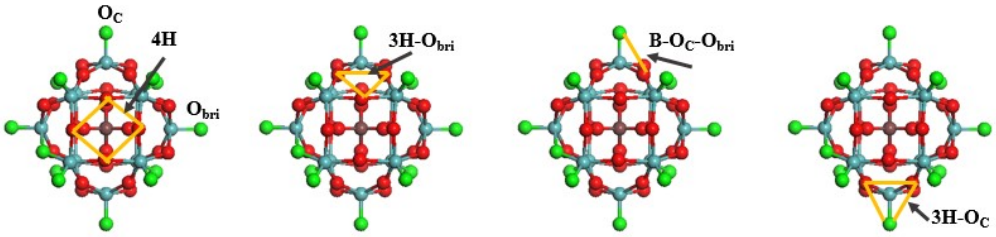


**Figure S1.** Optimized geometry of PMA with various possible coordination sites [1-2]. The green, red, carmine, and blue color represent corner oxygen ($O_t$), bridge oxygen ($O_{bri}$), phosphorus (P), and molybdenum (Mo) atoms, respectively (a) four-fold hollow site (4H); (b) 3-fold hollow site (3H-$O_{bri}$); (c) corner-bridge site (B-$O_c$-$O_{bri}$); and (d) three hollow corner site (3H-$O_c$) for metal atoms.

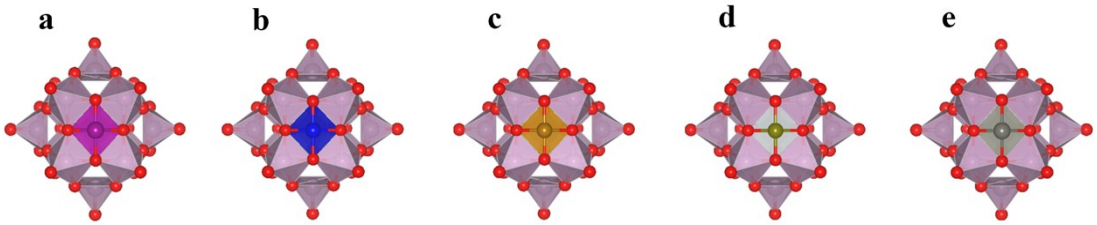


**Figure S2.** Optimized 3d-$TM_1$ (3d-$TM_1$= $Fe_1$, $Co_1$, $Ni_1$, $Cu_1$, and $Zn_1$) structures adsorbed at the four-fold hollow site (4H) on the PMA cluster.

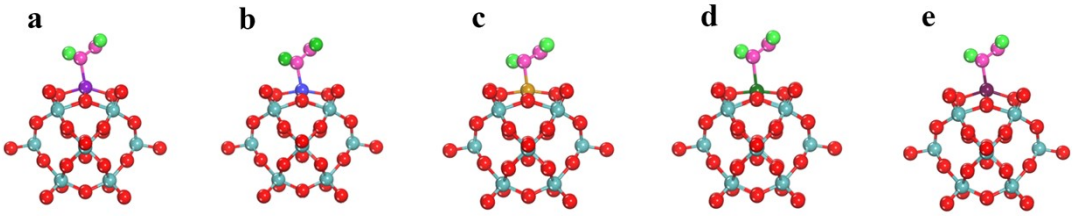


**Figure S3.** Optimized structures of $H_2O_2$ adsorbed on 3d-$TM_1$/PMA (3d-$TM_1$= $Fe_1$, $Co_1$, $Ni_1$, $Cu_1$, and $Zn_1$) clusters.

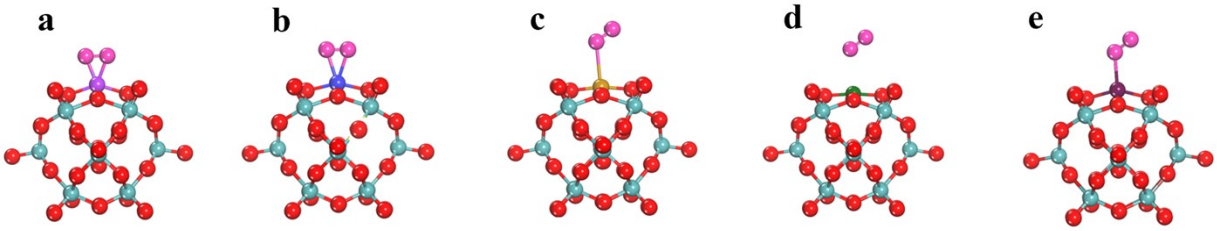


**Figure S4.** Optimized structures of $O_2$ adsorbed on 3d-$TM_1$/PMA (3d-$TM_1$= $Fe_1$, $Co_1$, $Ni_1$, $Cu_1$, and $Zn_1$) clusters.

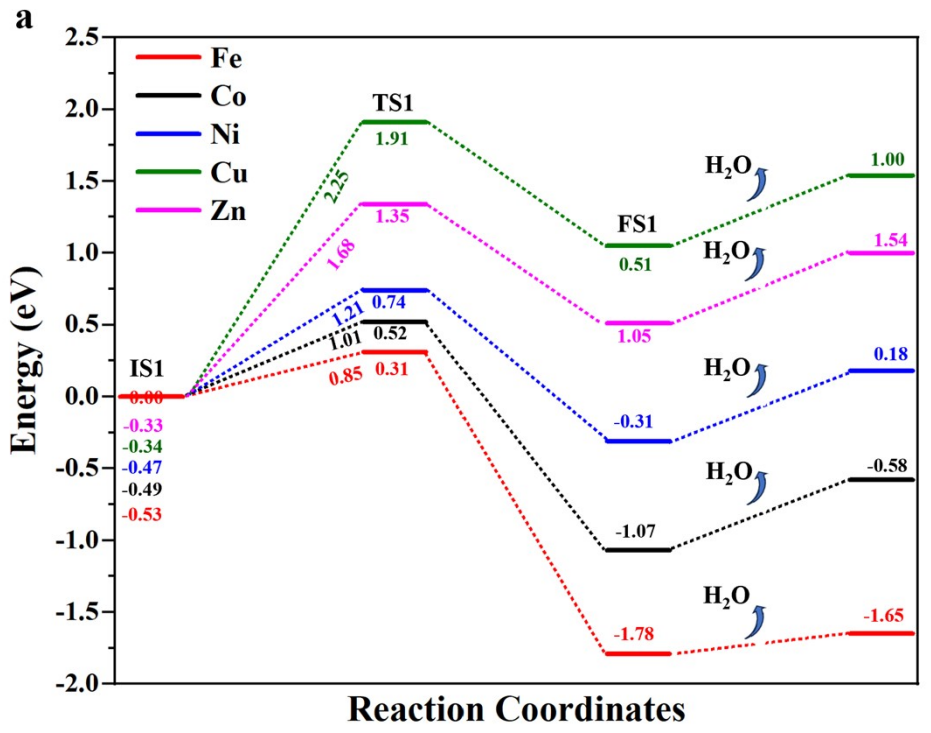
a
Fe
Co
Ni
Cu
Zn
TS1
1.91
2.25
1.35
1.68
0.74
1.21
0.52
1.01
0.31
0.85
IS1
0.00
-0.33
-0.34
-0.47
-0.49
-0.53
FS1
0.51
1.05
-0.31
-1.07
-1.78
H2O
1.00
1.54
0.18
-0.58
-1.65
Energy (eV)
Reaction Coordinates

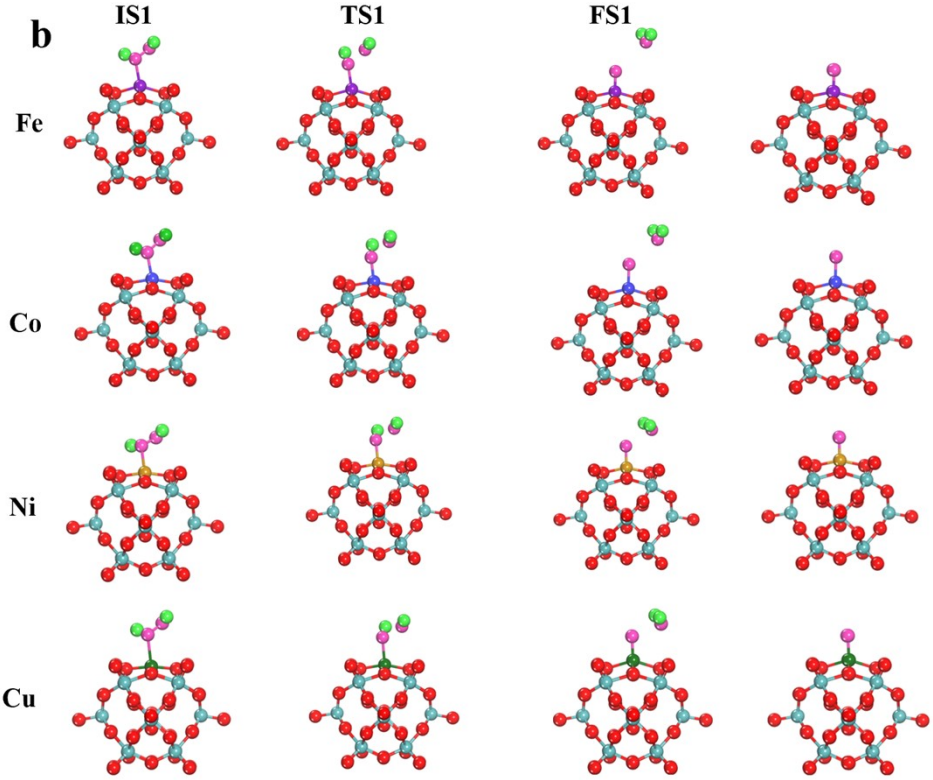
b
IS1
TS1
FS1
Fe
Co
Ni
Cu

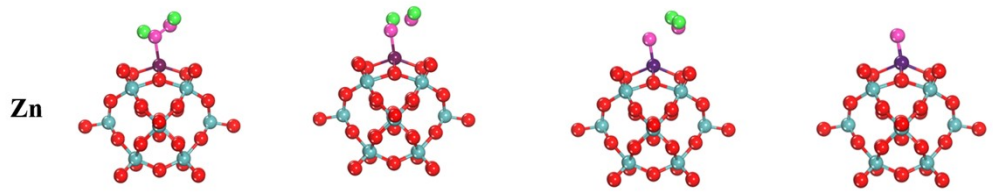


**Figure S5.** (a) Potential energy profile of the efficient decomposition of $H_2O_2$ on 3d-$TM_1$/PMA (3d-$TM_1$ = $Fe_1$, $Co_1$, $Ni_1$, $Cu_1$, and $Zn_1$), all DFT energies are in eV; (b) the optimized geometries of $H_2O_2$ decomposition on 3d-$TM_1$/PMA (3d-$TM_1$ = $Co_1$, $Ni_1$, $Cu_1$, and $Zn_1$).

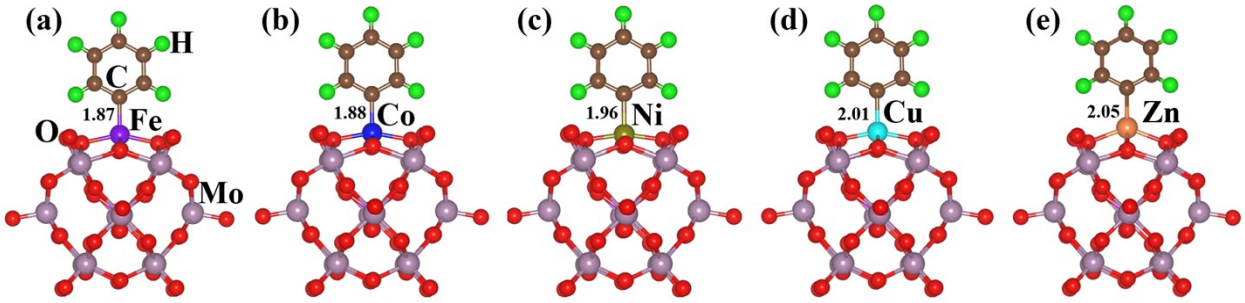


**Figure S6.** Optimized structures of benzene adsorbed on 3d-$TM_1$/PMA (3d-$TM_1$= $Fe_1$, $Co_1$, $Ni_1$, $Cu_1$, and $Zn_1$) clusters, respectively.

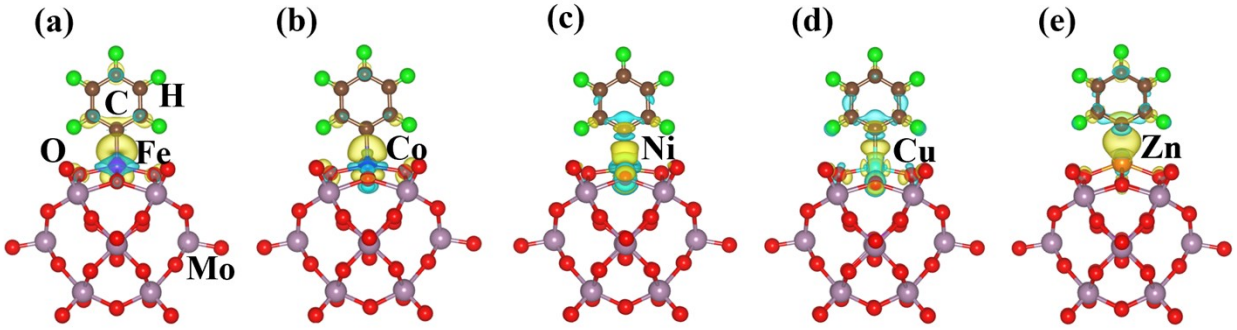


**Figure S7.** (a) Charge density plots for optimized structures of benzene adsorbed on 3d-$TM_1$/PMA (3d-$TM_1$= $Fe_1$, $Co_1$, $Ni_1$, $Cu_1$, and $Zn_1$) clusters, respectively.

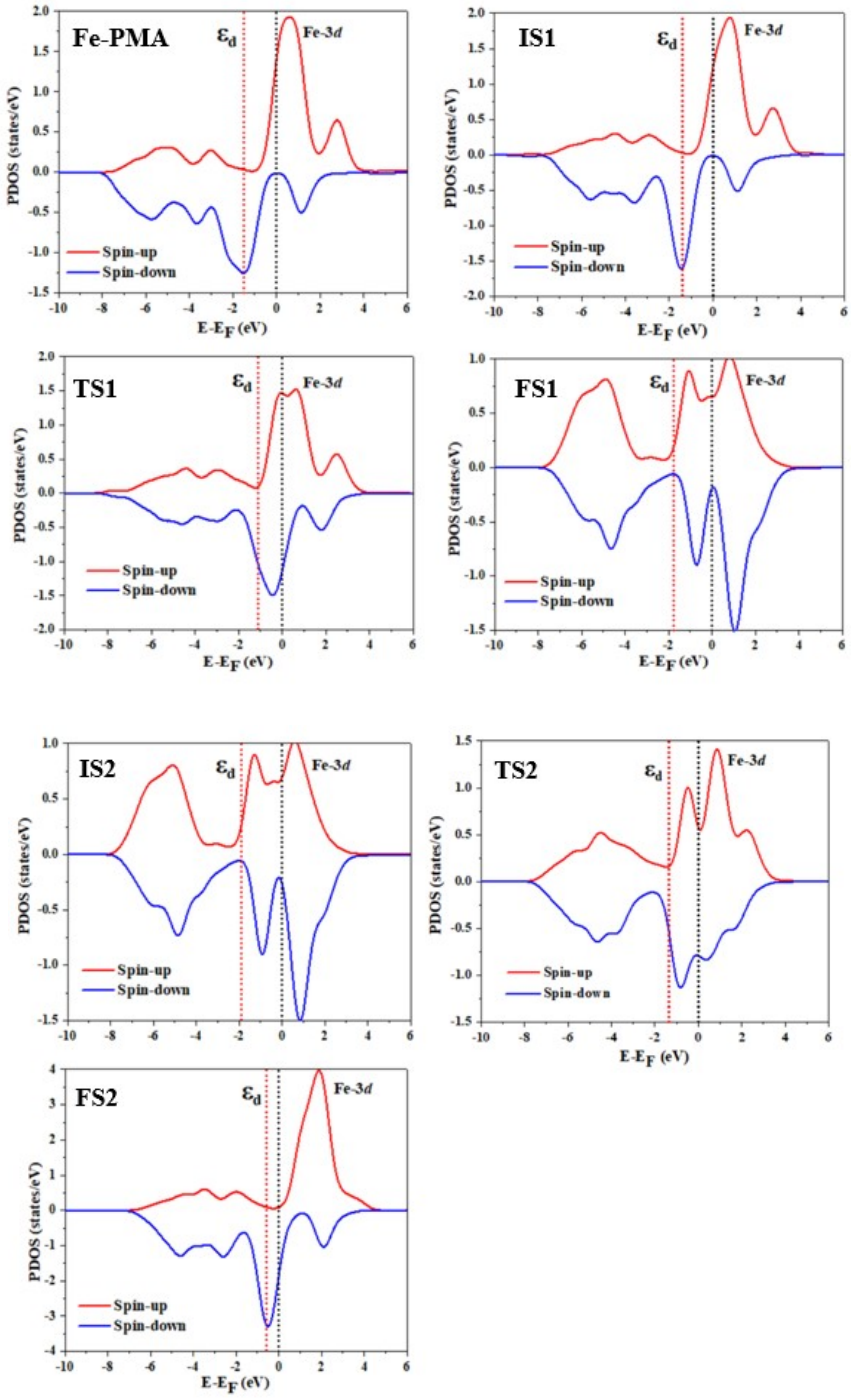


**Figure S8.** Spin-polarized partial density of states (PDOS) of all the elementary steps involved in the benzene oxidation to phenol reaction using $H_2O_2$ oxidizer projected on Fe-3*d* states. The Fermi level is set to be zero. The d-band center shows the change regarding the fluctuation in Fe-3*d* orbital in all the elementary steps near the Fermi level.

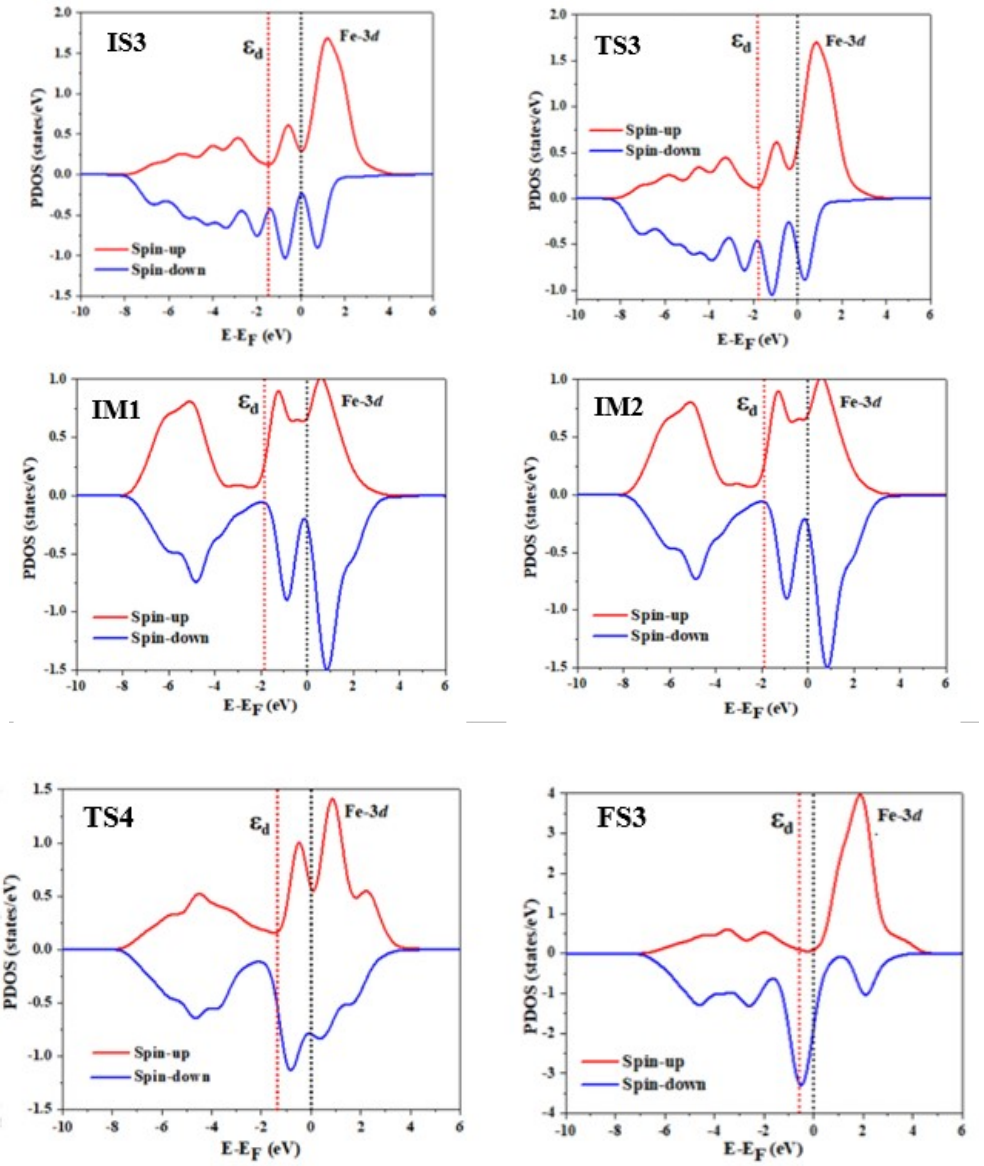


**Figure S9.** Spin-polarized partial density of states (PDOS) of all the elementary steps involved in the benzene oxidation to phenol reaction using $O_2$ oxidizer projected on Fe-3*d* states. The Fermi level is set to be zero. The d-band center shows the change regarding the fluctuation in Fe-3*d* orbital in all the elementary steps near the Fermi level.

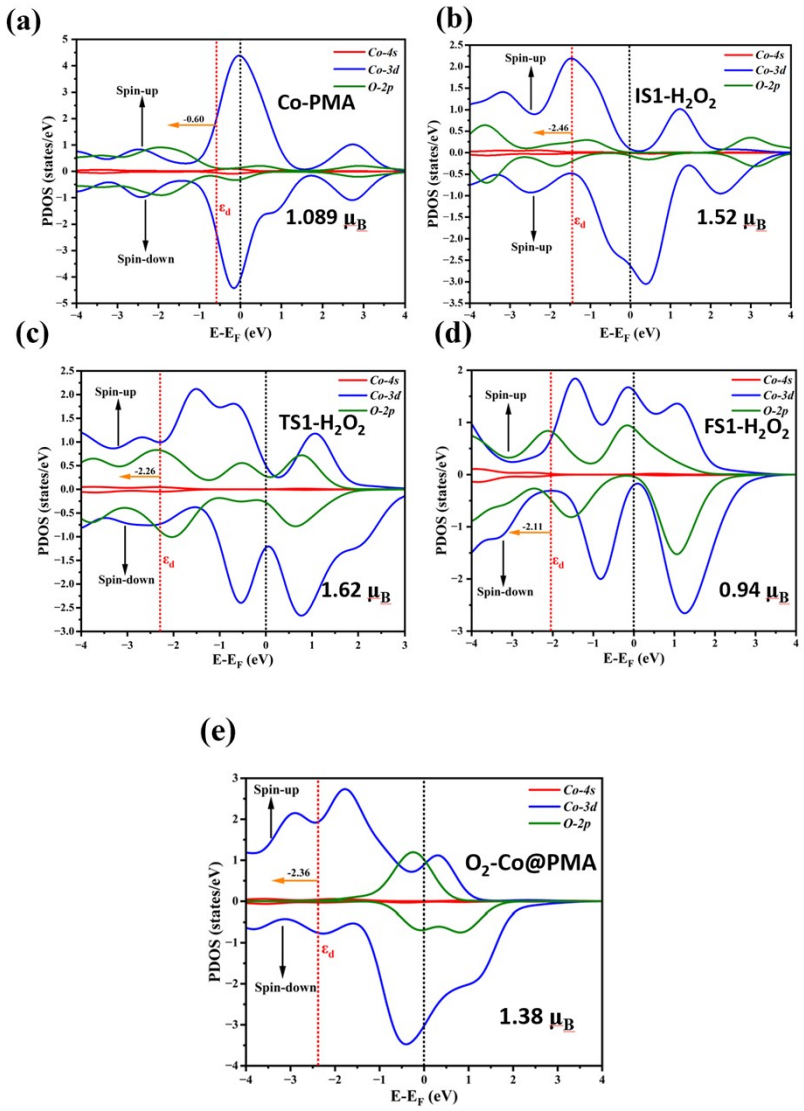


**Figure S10.** Spin-polarized partial density of states (PDOS) of $Co_1$/PMA (a), $H_2O_2$/$Co_1$/PMA (b-d), and $O_2$/$Co_1$/PMA (e), respectively. The Fermi level is set to be zero. The d-band center shows the change regarding the fluctuation in Co-3*d* orbital near the Fermi level.

**Explanation of Figure S10**

In the valence PDOS of $Co_1$/PMA near the Fermi level, the spin-up and spin-down distributions show less separation. This effect is attributed to a slight downward shift (more negative energy) of the spin-up Co states, likely stemming from Co magnetic properties. Co, with its partially filled d-orbitals, fosters interactions between spin-up and spin-down electrons, potentially causing the

observed shift in spin-up states. Comparing the spin effect, we note a trend of $Fe_1 > Co_1$, evident in both the magnitude of the spin effect and the simple d-band model. In summary, our exploration sheds light on the intricate spin configurations of the $Co_1$/PMA cluster, revealing $Co_1$ distinct behavior compared to $Fe_1$ and offering insights into magnetic phenomena and materials design.

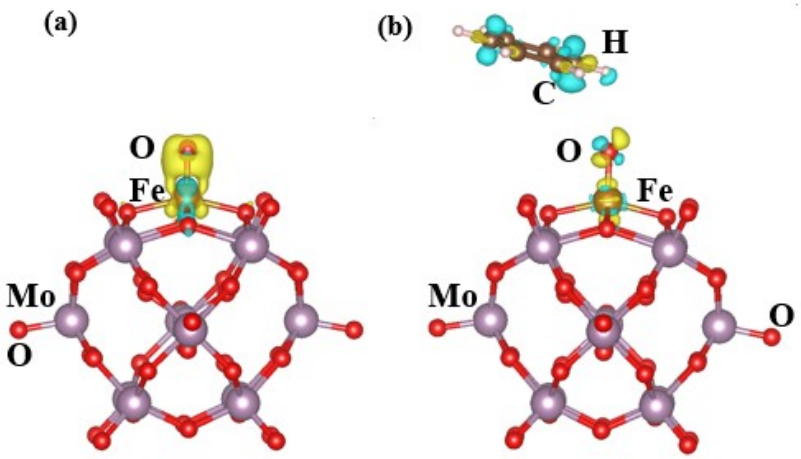


**Figure S11.** (a) Charge density plots for optimized structures of $OFe_1$-PMA; (b) and $C_6H_6$-OFe1-PMA.

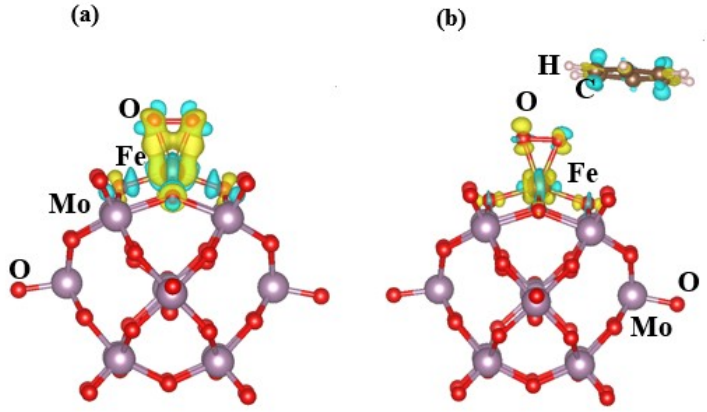


**Figure S12.** (a) Charge density plots for optimized structures of $O_2$Fe1-PMA; (b) and $C_6H_6$-$O_2$Fe1-PMA.

**Table S1.** Energy difference of adsorption energies of Fe adsorbed on PMA cluster by using different values of cutoff energy and k-points grids.

| Systems | 400 eV | 450 eV | 500 eV |
|---|---|---|---|
| $Fe_1$/PMA | -10.4732 | -10.4727 | -10.4724 |

Energy difference by using different k-points grid

| Systems | 1X1X1 | 3X3X3 | 5X5X5 |
|---|---|---|---|
| $Fe_1$/PMA | -10.4732 | -10.4787 | -10.4657 |

Our theoretical investigation suggests that employing a 400 eV cutoff energy and 1×1×1 k sampling point is suitable for studying the benzene oxidation reaction. This is supported by the calculated adsorption energies of $Fe_1$/PMA, which indicate that other cutoff energies such as 450 eV and 500 eV, along with 5 x 5 x 5 and 3 x 3 x 3 k sampling points, respectively, yield nearly identical values.

**Table S2.** Calculated P-O, Mo-$O_C$, Mo-$O_{bri}$, and $O_{bri}$-$O_{bri}$ (fourfold binding sites) bond lengths (Å) in isolated PMA and association with literature.

| Bond | This work | Past theories | Past experiments [1, 2] |
|---|---|---|---|
| P-O | 1.55 | 1.54, 1.55,1.58 | 1.54 |
| Mo-$O_C$ | 1.69 | 1.69,1.70 | 1.68 |
| Mo-$O_{bri}$ | 1.94 | 1.94,1.94,1.93 | 1.92 |
| $O_{bri}$-$O_{bri}$ | 2.71 | 2.68 2.72 | - |

**Table S3.** Binding site, calculated binding energies (eV), formation energies (eV), average bond lengths between the between the metal atoms and neighboring oxygen atoms (Å) and Bader charge [q(e)] of transition metal atoms (3d-$TM_1$ = $Fe_1$, $Co_1$, $Ni_1$, $Cu_1$, and $Zn_1$ adsorbed on PMA cluster.

| **Systems** | **Binding Site** | **$E_{bin}$/eV** | **Formation energies (eV)** | **Average Bond Length (Å)** | **q (e)** |
|---|---|---|---|---|---|
| $Fe_1$/PMA | 4H-site | -10.47 | -5.68 | 1.83 | 1.66 |
| $Co_1$/PMA | 4H-site | -10.44 | -4.84 | 1.82 | 1.38 |
| $Ni_1$/PMA | 4H-site | -9.40 | -4.51 | 1.83 | 1.35 |
| $Cu_1$/PMA | 4H-site | -7.44 | -3.90 | 1.84 | 0.61 |
| $Zn_1$/PMA | 4H-site | -5.46 | -4.50 | 1.93 | 0.84 |

**Table S4.** Adsorption energies of the $H_2O_2$ and $O_2$ molecule on 3d-$TM_1$ = $Fe_1$, $Co_1$, $Ni_1$, $Cu_1$, $Zn_1$/PMA cluster.

| Systems | $E_{ads}$ for | $E_{ads}$ for $O_2$ (eV) |
|---|---|---|

| | $H_2O_2$ (eV) | |
|---|---|---|
| $Fe_1$/PMA | -0.53 | -0.41 |
| $Co_1$/PMA | -0.49 | -0.13 |
| $Ni_1$/PMA | -0.47 | -0.23 |
| $Cu_1$/PMA | -0.34 | -0.04 |
| $Zn_1$/PMA | -0.33 | -0.18 |

**Table S5.** The calculated binding energy of $Fe_1$-PMA on different sites of the PMA cluster.

| Adsorbed Metal | Adsorption Sites | Binding Energy (eV) |
|---|---|---|
| **Fe** | **4-H** | **-10.47** |
| | 3H-$O_{bri}$ | -10.1 |
| | 3H-$O_c$ | -8.13 |
| | B-$O_c$-$O_{bri}$ | -7.56 |

**Table S6.** Adsorption energies of benzene molecule on 3d-$TM_1$ = $Fe_1$, $Co_1$, $Ni_1$, $Cu_1$, $Zn_1$/PMA clusters, respectivley.

| Systems | Adsorption Energy (eV) |
|---|---|
| $C_6H_5/Fe_1$/PMA | -1.62 |
| $C_6H_5/Co_1$/PMA | -2.04 |
| $C_6H_5/Ni_1$/PMA | -2.09 |
| $C_6H_5/Cu_1$/PMA | -0.79 |
| $C_6H_5/Zn_1$/PMA | -1.05 |

**Chemisorption of benzene on all studied $TM_1$ ($Fe_1$, $Co_1$, $Ni_1$, $Cu_1$, and $Zn_1$)**

According to results from Figure S6 and Table S6, $Ni_1$ exhibited the strongest adsorption energy of -2.09 eV, indicating a more chemisorptive interaction than the other metals. Conversely, $Cu_1$ displayed the weakest adsorption energy of -0.79 eV, suggesting a more physisorptive-like interaction. The bond length between metal and C of benzene decreases as increase the atomic size of metals from, $Fe_1$ to $Zn_1$, but there is no obvious change in adsorption geometries for benzene chemisorbed on the studied metals. This is rationalized by the fact that covalent bonds largely determine the local coordination for benzene at these substrates. Figure S7 presents the charge density plots for the optimized chemisorption structures. These plots reveal an increase in charge density between the metal and carbon atoms of benzene, indicating electron sharing and a more

covalent bond formation. Conversely, a decrease in charge density is observed between the metals and oxygen atoms of the PMA support, suggesting a weakening of the metal-support interaction upon chemisorption.

**References:**


[1] S. Wen, W. Guan, Y. Kan, G. Yang, N. Ma, L. Yan, Z. Su, G. Chen, *Phys. Chem. Chem. Phys.* **2013,** *15*, 9177-9185.

[2] S.-T. Zheng, G.-Y. Yang, *Chem. Soc. Rev.* **2012,** 41, 7623-46.